Ground-based observation of clusters and nucleation mode particles in the Amazon

Daniela Wimmer[1], Stephany Buenrostro Mazon[1], Hanna Elina Manninen[1,2], Juha Kangasluoma[1], Alessandro Franchin[1,3,4], Tuomo Nieminen[1,5], John Backman[6], Jian Wang[8], Chongai Kuang[8], Radovan Krejci[7], Joel Brito[9,10], Fernando Goncalves Morais[9], Scot Turnbull Martin[11], Paulo Artaxo[9], Markku Kulmala[1], Veli-Matti Kerminen[1] and Tuukka Petäjä[1]

[1]Department of Physics, University of Helsinki, Gustaf Hallströmin katu 2a, 00560, Helsinki, Finland
[2]European Organization for Nuclear Research (CERN), 1211 Geneva, Switzerland
[3]NOAA Earth System Research Laboratory (ESRL), Chemical Sciences Division, Boulder, CO, USA
[4]Cooperative Institute for Research in Environmental Sciences, University of Colorado Boulder, Boulder, CO, USA
[5]Department of Applied Physics, University of Eastern Finland, Post Office Box 1627, 70211 Kuopio, Finland
[6]Finnish Meteorological Institute, Atmospheric composition research, Erik Palménin aukio 1, 00560, Helsinki, Finland
[7]Stockholm University, Department of Environmental Science and Analytical Chemistry (ACES), 106 91 Stockholm, Sweden
[8]Environmental and Climate Sciences Department, Brookhaven National Laboratory, Upton, New York, USA
[9]Institute of Physics, University of São Paulo, de Fisica, Universidade de Sao Paulo, Rua do Matao 1371, CEP 05508-090, Sao Paulo, Brazil
[10]Laboratory for Meteorological Physics (LaMP), Université Clermont Auvergne, F-63000 Clermont-Ferrand, France
[11]School of Engineering and Applied Sciences, Harvard University Cambridge, Massachusetts 02138, United States of America

Correspondence to: Daniela Wimmer (daniela.wimmer@helsinki.fi)
Keywords: atmospheric ions, particle formation, rainforest, high-frequency rainfall

Abstract

We investigated atmospheric new particle formation (NPF) in the Amazon rainforest using direct measurement methods. To our knowledge this is the first direct observation of NPF events in the Amazon region. Previous observations in Brazil showed the occurrence of nucleation mode particles. Our measurements extended to two field sites and two tropical seasons (wet and dry). We measured the variability of air ion concentrations (0.8 – 12 nm) with an ion spectrometer between September 2011 and January 2014 at a rainforest site (T0t). Between February and October 2014, the same measurements were performed at a grassland pasture site (T3) as part of the GoAmazon 2014/5 experiment, with two intensive operating periods (IOP1 and IOP2 during the wet and the dry season respectively). The GoAmazon 2014/5 experiment was designed to study the influence of anthropogenic emissions on the changing climate in the Amazon region. The experiment included basic aerosol and trace gas measurements at ground, remote sensing instrumentation and two aircraft, capable of flying at different altitudes, probing the vertical layers over the Amazon.

The results presented in this work are from measurements performed at ground level at both sites. The inside the rainforest (T0t) site is located 60 km NNW of Manaus, mostly parallel wind to Manaus, and influenced by pollution about once per week. The pasture (T3) site is located 70 km downwind from Manaus and influenced by the Manaus pollution plume typically once per day or every second day, especially in the afternoon. No NPF events were observed inside the rainforest (site T0t) at ground level during the measurement period. However, rain-induced ion and particle bursts (hereafter, "rain-events") occurred frequently (643/1031 days) at both sites throughout the year but most frequently during the wet season. During the rain-events, the ion concentrations in three size ranges (0.8-2 nm, 2-4 nm and 4-12 nm) increased up to the order of 10^4 - 10^5 cm^{-3}. This effect was most pronounced in the intermediate and large size range, where the background ion concentration was about 10 – 15 cm^{-3}, as compared with 700 cm^{-3} for the cluster ion background.

We observed 8 new particle formation (NPF) events at the pasture site during the wet season. We calculated the growth rates and formation rates of neutral particles and ions for the size ranges 2-3 nm and 3-7 nm using the ion spectrometer data. The observed median growth rates are 0.8 nmh^{-1} and 1.6 nmh^{-1} for 2-3 nm-sized ions and particles respectively, with larger growth rates (13.3 nmh^{-1} and 7.9 nmh^{-1}) in the 3-7 nm size range. The measured nucleation rates are in the order of 0.2 $cm^{-3}s^{-1}$ for particles and 4-9*10^{-3} $cm^{-3}s^{-1}$ for ions. There was no clear difference in the sulfuric acid concentrations between the NPF event days and non-event days (~9*10^5 cm^{-3}). The two major differences between the NPF days and non-event days were a factor of 1.8 lower condensation sink on NPF event days (1.8*10^{-3} s^{-1}) compared to nonevents (3.2*10^{-3} s^{-1}) and different air mass origins. To our knowledge, this is the first time that results from ground-based sub-3 nm aerosol particle measurements have been obtained for the Amazon rainforest.

1 Introduction

Globally, atmospheric new particle formation (NPF) and growth has been estimated to account for a major, if not dominant, fraction of atmospheric cloud condensation nuclei (Merikanto et al. 2009, Wang and Penner, 2009, Yu and Luo, 2009, Dunne et al., 2016, Kulmala et al., 2016). The formation of atmospheric nanoparticles is a multi-stage process, in which stable clusters form from gas phase precursors followed by the activation of these clusters and further growth (Kulmala et al. 2014). Although, atmospheric NPF is occurring frequently in many environments (e.g. Kulmala et al. 2004, Manninen et al. 2010), the Amazon basin is one of the locations where the initial steps of the formation of nanoparticles had not been previously observed from ground - based measurements (Martin et al, 2010a).

In the Amazon, emissions and oxidation of volatile organic compounds (e.g. Lelieveld et al. 2008), aerosol activation to cloud droplets, and eventually rain formation, are tightly connected with synoptic processes, such as deep convection for example (Lelieveld et al. 2008, Wang et al., 2016). Aerosol concentrations in the Amazonian atmosphere are rapidly changing as a result of deforestation and the associated biomass burning and economic development in the Amazon region (Martin et al. 2016, Artaxo et al., 2013). The Manaus metropolis (population 2 million) is the capital of the state of Amazonia, Brazil, surrounded by the largest rainforest on Earth (Martin et al, 2017), as shown in Fig 1. The measurements discussed in this paper took place at two different locations in the Amazon rainforest: a pasture site 70 km downwind from Manaus (T3; Martin et al., 2016); and a site within the rainforest, mostly unaffected by Manaus pollution (T0t; Martin et al., 2010b). The sites are described in more detail in section 2.1.

Depending on the wind direction, these sites can represent (i) one of the most natural continental locations on Earth, or (ii) a location affected by both polluted and clean air masses (Martin et al., 2016). The complexity of the mixture of trace gases and aerosol population make the Amazon rainforest an interesting place to study. During most of the wet season the Amazon basin is one of the cleanest continental regions on Earth (Andreae, 2007; Martin et al., 2010a, Artaxo et al., 2013, Andreae et al., 2015). During the dry season, the Amazon basin is highly influenced by anthropogenic emissions mostly from biomass burning. Additionally, our study region experiences frequent high-intensity precipitation episodes.

The primary goal of this paper was to investigate the occurrence of new particle formation (NPF) and growth in the Amazon region, and to quantify the role of ions and aerosol particles in this process

2 Methods

The measurements discussed here were obtained from two different locations: inside the Amazon rainforest (2011-2014) and in the vicinity of the rainforest at a pasture site (2014). The measurements inside the rainforest at site T0t were performed over 3 years from September 2011 to January 2014. The second measurement site (T3) was part of the Green Ocean Amazon (GoAmazon2014/5) Experiment (Martin et al., 2016). The GoAmazon2014/5 Experiment was performed from January 1, 2014 to December 31, 2015. The experiment included two intensive operation periods (IOP1 and IOP2). IOP1 extended from February 1, 2014 to March 31, 2014 and IOP2 from August 15, 2014 to October 15, 2014 (Martin et al., 2016). The experiment was designed to study the perturbation in cloud and aerosol dynamics in the Amazon rainforest by the Manaus emissions. The ion spectrometer measurements were conducted from January 28 to October 13, 2014. Figure 1 shows the locations of both measurement sites. Table 1 shows an overview over the available dataset presented in this study.

2.1. Measurement sites

2.1.1 Measurement site inside the rainforest

The T0t ecological reserve (Martin et al, 2010b) is a terrestrial ecosystem science measurement site located 70 km NNW of the Manaus metropolis in the central region of Brazil (2.609°S, 60.2092°W). Two major rivers, the Solimoes and the Rio Negro merge together in Manaus to become the Amazon river. The city of Manaus is the capital of the state of Amazonia, Brazil, with more than 2 million inhabitants (IBGE, 2015). It is the seventh biggest city in Brazil and is surrounded by forest for 1500 km in all directions (Martin et al., 2016).

T0t is surrounded by a dense rainforest. The rainforest canopy is homogeneous with an average height of 30 m. T0t is influenced by anthropogenic pollution about once per week (Martin et al., 2010b supplementary material, Thalmann et al, 2017, de Sa et al, 2017). Otherwise, the location of the T0t site allows the characterization of an almost completely undisturbed natural environment (Martin et al, 2016).

2.1.3 Open pasture measurement site

A Mobile Facility from the Atmospheric Radiation Measurement (ARM) Program (Mather et al., 2014) of the United States Department of Energy was deployed at the T3 site close to Manacapuru, about 70 km downwind of the city of Manaus (3.2133°S, 60.5987°W), and included an ARM Mobile Aerosol Observing System (MAOS). The site is an open pasture site, where the Manaus pollution plume regularly intersects. Due to the site location, T3 is influenced by the Manaus pollution plume typically once per day or every second day, especially in the afternoon (Martin et al., 2010b supplementary material, Thalmann et al, 2017, de Sa et al, 2017). The site also hosted numerous instrument systems from other GoAmazon2014/5 participants (Martin et al., 2016).

2.2 Instrumentation

2.2.1 Neutral cluster and Air Ion Spectrometer (NAIS)

A Neutral cluster and Air Ion Spectrometer (NAIS; Manninen et al., 2016) was used to determine the early stages of atmospheric nucleation and subsequent growth. The NAIS measures the mobility distributions in the range 3.2 – 0.0013 $cm^2\ V^{-1}\ s^{-1}$, which corresponds to a mobility equivalent diameter range of 0.8 – 42 nm. The ion and neutral particle size distributions are measured in three different stages: ion, particle, and offset. The NAIS consists of two parallel cylindrical DMAs (Differential Mobility Analyzers), one for classifying negative ions and the other for positive ions. When in ion mode, corona chargers and electrostatic filters are switched off to allow only naturally charged ions into the DMA. During the particle mode, the particles are charged by a corona charger in order to be detected by the DMA. The inlet flow into the NAIS is 60 liters per minute (Lpm), whereas the sample and the sheath flows of the DMAs are 30 and 60 Lpm, respectively. The NAIS time resolution was set to 5 min, which includes a full measurement cycle of negative ions, positive ions, and total particles. The NAIS instrument and calibration are described in more details in Asmi et al. (2009), Wagner et al. (2016) and Manninen et al. (2016). The accuracy of the ion concentration of the NAIS was estimated to be 10 - 30%, which was mainly due to flow rate uncertainties (Manninen et al., 2016; Wagner et al., 2016). The electrometers measure a current which can be transformed into particle concentrations. If concentrations are low, the noise can be quite high and can result in negative concentration values. The environmental conditions in the Amazon are very challenging for NAIS measurements, especially the high relative humidity (RH). To reduce the NAIS sampling RH, an electric heater was installed at the inlet to heat the air being sampling to 60° C to evaporate some water before entering the instrument.

The NAIS was placed inside a hut at the T0t site, sampling at 2 m above the ground level. In January 2014, the NAIS was moved to the T3 site where it was placed outside under a roof. The sampling setup was the same at both sites. The measurements were not continuous through these 3 years. In total 736 days of neutral particle data and 718 days of ion data were taken at both sites together (see Table 1).

2.2.2 Particle Size Magnifier (PSM)

A Particle Size Magnifier (PSM; Airmodus A09; Vanhanen et al., 2011) was used to determine aerosol particle concentrations at sizes below 3 nm. A PSM is a mixing-type condensation particle counter (CPC), in which the aerosol is turbulently mixed with air saturated with diethylene glycol (DEG). DEG only grows the particles to about 90 nm, so the PSM system consists of a second stage, where the particles are grown to optically detectable sizes. The 50% activation diameter of the instrument can be varied across a size range of 1–4 nm in mobility diameter (Vanhanen et al., 2011) by changing the mixing ratio of the saturator and sample flow. At GoAmazon2014/5, the PSM was used in a scanning mode in which the saturator flow is continuously changing, altering the cut-off diameters between 1 and 4 nm. One scan takes 4 min and the system was setup to do one upscan, followed by a downscan. Due to the challenging measurement conditions, the size-resolved data was not used in this analysis.

Prior to the deployment during the GoAmazon2014/5 campaign, the PSM system was equipped with an inlet system specifically designed to decrease the relative humidity of the sample without disturbing the sample itself and maintain high flow rates (10 Lpm) until the actual sampling to minimize diffusion losses. The inlet system comprises a core sampling probe combined with a sintered tube. The core sampling probe consists of two cylindrical tubes with different outer diameters (10 mm and 6 mm). The larger diameter of the outer tube allows a total laminar flowrate of up to 10 Lpm, to minimize diffusional losses. The inner tube is directly attached to the PSM with an airflow of 2.5 Lpm. The excess airflow is discarded into an exhaust line (Kangasluoma et al., 2016). Downstream of the core sampling line is a sintered tube where dry pressurized air is introduced.

The water molecules in the sample flow are pushed towards the outer walls of the sintered material by diffusion, drying the airflow.

Laboratory studies have shown that RH can drastically affect the PSM counting efficiency (higher sensitivity at smaller sizes at higher RH; Kangasluoma et al, 2013, Iida et al, 2009). Since the aerosol in Brazil was expected to be composed of mostly organic species, the PSM with the inlet was calibrated using limonene and its oxidation products (Kangasluoma et al, 2014) as a test aerosol. The resulting lowest PSM cut-off diameter was 1.5 nm (±0.3 nm), where the uncertainty was estimated as a combination of the calibration uncertainty and the influence of the ambient RH on the PSM cut-off diameter. In total, 38 days of data obtained during the dry season were used.

2.2.3. Supporting instrumentation at both sites

At T0t, the submicron aerosol number size distributions and total particle number concentrations were monitored with a DMPS system (Aalto et al., 2001) and a CPC. The CPC time resolution was 1 minute, with a 50% cut-off size of about 6 nm. The DMPS measured number size distributions over the mobility diameter range of 6 – 800 nm (Backman et al., 2012), and a complete size distribution was obtained every 10 minutes. The DMPS system was designed so that during the 10-minute measurement cycle, size-segregated aerosols were measured for 8 minutes, and for the remaining 2 minutes, total particle number concentrations were measured with the CPC directly using a bypass valve. The transmission at 4 nm of the inlet used the AMAZE-08 (Martin et al., 2010b) experiment was 50%. The diffusion losses are an exponential function of the size of the aerosol particles. Above a size of 10 nm, the diffusion losses in the current setup were not important anymore. For the measurements reported here, a similar setup with a 60 m sampling line was used. The DMPS data should be used in a qualitative rather than quantitative manner as the losses due to diffusion in the sampling line are not precisely known and therefore not considered. In addition to the ion spectrometer measurements, the measurement hut hosted a Vaisala system (WXT-520) for acquiring meteorological parameters.
The auxiliary data from the T3 site, presented in this manuscript includes measurements from an ultrafine CPC, with a 50% activation diameter of 10 nm and an SMPS with a lower cut-off of 20 nm. The meteorological data was retrieved from a Vaisala system (WXT-520). Those datasets are available at the ARM data browser.

2.3 Measurement periods: wet and dry season

The differences in the tropical seasons present contrasting environmental conditions (Martin et al., 2016, Artaxo et al., 2013). In our manuscript, we follow Artaxo et al. (2013) and define the wet season in the Amazon as January to June, and the dry season as July to December.

Anthropogenic influence in the Amazon region is mostly dominated by biomass burning emissions, which are strongest during the dry season. The most intense biomass burning and atmospheric perturbations take place at the southern and eastern edges of the forest (Brito et al., 2014), however, their transport impacts the whole basin. During the wet season, Manaus emissions are the main anthropogenic influence on the aerosol population in the Amazon region (Andreae, 2007; Martin et al., 2010a). During the dry season, the wet deposition decreases whereas the condensation sink increases. That leads to an overall increase in aerosol concentration in the accumulation mode of about one order of magnitude even in remote areas (Artaxo et al., 2013).

The planetary boundary layer development also displays a strong diel behavior, with a stable nocturnal layer and strong vertical mixing during daytime. The vertical transport is enhanced in strong convective situations when particles are lofted and entrained into the free troposphere. The stable nocturnal layer, on the other hand, traps the emissions near the surface; the impact can be more pronounced during the dry season as biomass burning usually starts at midday and continues into evening hours (Martin et al, 2010a). The boundary layer development is also different for the two different measurement sites, as the boundary layer develops more rapidly over the pasture area, with more efficient vertical mixing compared to the site enclosed by rainforest.

2.4 Data analysis

All the available data from the NAIS were cleaned for a potential instrumental noise. The cleaning process was done visually using the particle and ion size distributions as surface plots. Based on this initial screening, the decision was made whether one or more of the electrometers were reliable or not. The non-reliable data were removed based on the guidelines introduced by Manninen et al. (2010). The NAIS data turned out to be unreliable during the measurements presented here mostly in the size range above 15 nm. Therefore, we decided to show data for the sizes up to 12 nm only in our analysis.

We observed an increase in the concentrations of the cluster ions in the NAIS starting from October 7, 2013 to January 21, 2014. By investigating the raw data files, this drift was observed to be due to too low currents in the sheath air filters. The sheath air filters are electrical filters, using corona needles to neutralize all the remaining ions, which leads to an over-estimation of the ion concentrations. A correction factor of 1.8 was applied to account for this problem in the 4 smallest size channels of the NAIS (0.8-1.25 nm) for the data taken at the T0t site after the drift was observed.

This increased level in the positive polarity of the natural ions continued when the NAIS was re-deployed at the T3 site. The cause was the same (too low a current in the sheath air filters). We consider the positive polarity of the natural charged ions in the NAIS at the T3 site unreliable, therefore the data, regarding the absolute concentrations, using the positive channel for the T3 site is not shown in this study. Additionally, the ion data from September 9-26, 2014 at the T3 site was considered unreliable and also excluded from our analysis.

Rain-induced ion events were selected as days, when an ion burst coincided with the onset of precipitation. The median and the maximum (99^{th} percentile) ion concentrations were calculated during periods when the rain intensity was >0 mm h^{-1}. In case of more than one rain-event per day, two separate rain-events were classified as such, if the start of the second one occurred more than an hour after the end of the first one. Any fluctuations in the rain intensity for a time period shorter than 1 hour were considered to be part of a single rain-event. At T0t, we classified 962 rain-events and at T3, 221 rain-events.

The new particle formation event analysis from the ion spectrometer data, including the event classification and formation and growth rate calculations, followed the already well-defined guidelines (Kulmala et al., 2012). In the data analysis, the first step was to classify all available days into NPF event and non-event days according to methods introduced earlier by Hirsikko et al. (2007) and Manninen et al. (2010). The days which do not fulfill the criteria of an event or non-event day, are categorized as undefined days, however, there were no days classified as undefined in this study. The classification was performed manually through a visual inspection of daily contour plots of particle number size distributions. The second step in the analysis was to define the characteristics related to each NPF event, such as the particle growth rate (GR) and formation rate (J). The GRs were calculated for two different size bins (2-3 nm and 3-7 nm in particle diameter) using both ion and neutral particle data from the NAIS. The particle growth rate was determined by finding the times at which the maximum concentrations of ions/particles in each of these size ranges occurred. A fit between the points was then applied to determine the growth rates. The particle formation rate was determined for the lower end of each size bin (2 and 3 nm) by considering the growth rates, the condensation sink, and the coagulation sink.

3 Results

All the times mentioned below are local Manaus time (LT), which is Coordinated Universal Time (UTC) –4 h.

3.1 Number concentrations of ions and particles at the two sites

An overview of the observed number concentrations of ions and particles together with the ambient meteorological conditions at the two measurement sites is presented in Table 2. We divided the measured ions and neutral particles into three sub-size ranges: cluster size-range (0.8 - 2 nm), intermediate size-range (2 - 4 nm), and large size-range (4 - 12 nm). Defining the lower and upper limits of the intermediate ion size range varies in the scientific literature (see Hirsikko et al., 2011 and references therein). The definition of using 2-4 nm as intermediate size-range allows for differentiating between atmospheric new particle formation events and non-events when using ion measurements (Leino et al., 2016).

When comparing the two measurement sites, the most apparent differences are, the almost factor of 3 lower intermediate negative ion concentrations at the T3 site compared to the T0t site (6 cm^{-3} wet (T3), 5 cm^{-3}dry (T3); 17 cm^{-3} wet and dry (T0t)). By contrast, the large-sized ion concentrations are about a factor of 2 higher at the T3 site compared to the T0t site (20 cm^{-3} wet (T3), 12 cm^{-3} dry

(T3); 8 cm^{-3} wet and dry (T0t)). Also, the intermediate and large-sized neutral particles are by about a factor of 3 higher at the T3 compared to the T0t site.

The environmental variables were relatively similar between the two sites, with higher temperatures and lower RH at the T3 site. The wind directions at both sites vary from the wet to the dry season. At T3 during the wet season, the air masses arrive from 115° N and 95° N during the dry season. At T0t the wind direction changes from 94° during the wet season to 105 °N during the dry season (see Table 2).

3.1.1 Inside rainforest site (T0t)

At the T0t site, the cluster ion concentrations are very comparable for the wet and the dry season (856 cm^{-3} and 952 cm^{-3}) for negative cluster ions. Positive cluster ion concentrations are much lower on the other hand, but also comparable for both seasons (549 cm^{-3} and 537cm^{-3}). These values are comparable to those found in several other locations (eg. urban Paris, Dos Santos et al. 2015; coastal Mace Head, Vana et al. 2008 and Finokalia, Kalvitis et al. 2012; Puy de Dome, Rose et al. 2016).

The ion concentrations in the intermediate size range (2-4 nm) are a factor of 2 higher (17 (-) wet, 34(+) wet; 17 (-) dry, 34 (+) dry). The ion concentrations in the large size range of 4 – 12 nm are the same in both polarities and both seasons (8 cm^{-3}). Neutral particle concentrations are higher in the intermediate (2-4 nm) compared to the large (4-12 nm) size range, but are very similar in the wet and the dry season.

The characteristics of the wet and the dry season in the Amazon (Rissler et al. 2006, Martin et al. 2010a) can be observed in the concentrations of the negative ions at the T0t site (Figure 2). The negative ion concentrations are decreasing from April to September and increasing between September and February. Most likely, the local biomass burning during the dry season increases the ion concentrations. During the wet season, their concentrations are decreased most likely due to wet deposition and reduced source strengths.

We observed a similar diel pattern for both the wet and the dry season for the neutral particles as shown in Figure 3. The concentrations in both size ranges increase at around 06:00 – 09:00 during the wet season. This effect is less pronounced in the dry season. A clear decrease in neutral particle concentrations during evening times (after 17:00) can be observed.

3.1.2. Pasture site (T3)

As shown in Table 2, typically, cluster ion concentrations at the T3 site were higher during the wet (1300 cm^{-3}) than the dry season (890 cm^{-3}). Similar high ion concentrations have been reported in an Australian rainforest in Tumbarumba (Suni et al. 2008) and in a wetland site in Abisko (Svennigsson et al., 2008). Those experiments showed concentrations of ~2400 (1700) cm^{-3} for negative (positive) ions. The median negative ion concentrations in two size ranges (2 - 4 nm and 4 - 12 nm) are very similar during the wet (6 cm^{-3}, 20 cm^{-3}) and the dry season (5 cm^{-3}, 12 cm^{-3}). The neutral particle concentrations are also very similar in both seasons at the T3 site. The median total concentrations measured by the ultrafine MAOS CPC (>10 nm) are more than a factor of 2 higher in the dry season than in the wet season (928 cm^{-3} versus 2000 cm^{-3}). This difference is most likely due to the enhanced biomass burning during the dry season. The average temperatures and the average relative humidity are very similar in both seasons.

The PSM measurements were performed during the dry season only. In total, 38 days of PSM data were included in this study and the results are shown in Figure 8. The PSM was used in scanning mode but, due to the challenging environmental conditions, only data measured at the highest supersaturation (total particle concentration at >1.5 nm) is shown.

The PSM data shows a similar diel pattern as the cluster ion concentrations measured by the NAIS (see Fig. 9), with higher median concentrations observed during the early morning (03:00-06:00), a dip in concentrations during the early afternoon (12:00-15:00), and then elevated median concentrations again in the evening (18:00-24:00). This could be explained by the Carnegie curve (Harrison, R. G. and Carslaw, K. S., 2003), which manifest a diel variation in the ionospheric potential.

3.2 Rain-induced ion formation events

While no NPF events were observed within the rainforest at site T0t, rain-induced ion burst events (hereafter, rain-events) were common and observed during 264 out the 384 measurement days. Since multiple rain episodes could occur in a single day, each rain-event was investigated separately, giving a total of 962 rain-events at T0t site and 221 at the T3 site.

Figure 4 shows an example of multiple rain-events that took place during January 24, 2013 (wet season). Negative ion concentrations in the cluster size range of 0.8 – 2 nm increased during the precipitation from about 1000 cm^{-3} to 1500 cm^{-3}. The positive cluster ion concentrations on the other hand decreased during the precipitation from 1000 cm^{-3} to about 500 cm^{-3}. The intermediate (2 - 4 nm) ion concentrations increased for both polarities, although the increase was more pronounced for the negative intermediate ions. In the intermediate size range, the concentrations of negative ions reached up to 3000 cm^{-3}, while during the same precipitation event, the positive intermediate ion concentrations only increased to 200 cm^{-3}.

A similar feature for 2-8 nm-sized negative ions during rain-events has also been reported for an Australian rainforest (Suni et al. 2008). During precipitation, positive ion concentrations increased only in the 3-7 nm size range and decreased in the 1-3 nm size range. Rain-induced bursts are thought to be a result of a balloelectric effect, in which splashing water produces intermediate ions such that the negative ions are smaller in size than the positive ions (Horrak et al., 2005, Hirsikko et al., 2007, Tammet et al., 2009). The duration of the 962 rain-events varied from a couple of minutes to 22 hours, with over half the rain-events lasting for two hours or less. The statistics of the rain-event frequency from the T0t measurement site are shown in Figure 5. The bars show the mean number of days with and without rain and the black line shows the median total average precipitation per month. The Figure shows that rain-events occur in both seasons. The number of days without rain increases during the dry season (July to December) as defined in Artaxo et al, 2013.

Figure 6 shows the relationship between the maximum negative ion concentration and median rain intensity during each rain-event. While no clear correlation between these two quantities was found, some specific features are apparent: at the site within the canopy (T0t), the highest cluster ion and intermediate ion concentrations occurred almost entirely in correlation with rather strong rain intensities, whereas at the pasture site (T3) almost no increase in negative ion concentrations in any size range during precipitation periods could be observed.

Rain-events were also evident in the total particle concentration measured by the NAIS, as depicted in Figure 7. In this example, the rain intensity peaks twice, about 40 mm h^{-1} at ~09:00 followed by a second peak of 10 mm h^{1} at ~11:00. The ion and particle concentrations measured by the NAIS increase and decrease almost simultaneously with the increase in the precipitation rate. Additionally, the DMPS data showed an appearance of nucleation mode particles between 6 and 10 nm also following the onset of rain. The DMPS was sampling at a height of 60 m, which is well above the rainforest canopy. The concentration of 6-10 nm size particles increased to ~20 cm^{-3} during the rain-event, while remaining below 5 cm^{-3} throughout the rest of the day. The 10-20 nm size particle concentration first showed a decrease followed by a slight increase up to ~35 cm^{-3}, peaking later than the short-term increase seen for 6-10 nm size particles. The appearance of 6-10 nm size particles and their peak concentration could present a similar scenario as observed in Wang et al (2016) of small particles brought down from the free troposphere. Wang et al. (2016) reported the production of small aerosol particles as a result of new particle formation at cloud outflow region, with further transport within the boundary layer via strong convection during precipitation events in the Amazon. Wang et al. (2016) noted that the <20 nm particle concentrations decreased very rapidly. We suggest the process that we observe to be a local one, as the production of ions was observed to only last for the duration of the precipitation.

3.3 New particle formation events at T3

We observed no NPF events during the dry season. During the wet season, on 9% of the days, we did observe NPF events. A similar event frequency has been observed in the Finnish boreal forest environment during autumn for example (Kontkanen et al., 2017). An earlier study by Backman et al. (2012) showed that in the metropolitan area of São Paulo (population 20 million), Brazil, NPF events occurred on 11% of the days. Zhou et al. (2002) observed an ultrafine particle mode in central Amazonia on 18% of the days.

We selected all eight NPF event days to characterize the behavior of ions and aerosol particles during the bursts of particle formation. A comparison of the diel cycle for particles and ions between NPF and non-event days is shown in Figure 9. The cluster ions showed a clear diel cycle with higher concentrations in the morning and evening for both NPF and non-event days. An increase in the concentration of the intermediate and large ions (2-4 nm and 4-12 nm) occurred during NPF event days, which is due to the growth of the ions from the cluster ion size range (0.8-2 nm). The intermediate neutral particle concentration increased at around 09:00, suggesting an onset of NPF after sunrise when the boundary layer begins to grow and turbulent mixing starts. On non-NPF days these particles showed highest concentrations after sunrise (06:00) and sunset (18:00). The total particle concentration measured by the MAOS CPC showed a clear concentration increase on NPF-event days, starting from 10:00, which clearly indicates that the particles had grown from smaller sizes below the 10 nm detection limit of the MAOS CPC. No clear diel pattern in the MAOS CPC measurements was visible on non-event days.

The type of NPF events that we observed are likely of regional nature, requiring relatively homogeneous air masses for at least a few hours (Vana et al., 2004; Manninen et al., 2010). The most likely explanations why no new particle formation events were observed at the T0t site are: (i) either the lack of SO_2 sources for forming sulfuric acid or (ii) that the sampling at the less polluted T0t site was performed within the rainforest, where mixing with the atmospheric boundary layer above is hindered. The gaps, or fluctuations, in the usually distinct NPF shape in time-size-concentration plots could be caused by some degree of heterogeneity in the measured air masses. All NPF events occurred during daytime, starting at around 08:00 - 09:00. Sunrise takes place at 06:00 in the Amazon basin. All NPF events also occurred during the wet season, which might be due to the lower condensation sink at this time of the year, as shown in Table 1. The median sulfuric acid concentrations as measured by a quadrupole HOx CIMS (Martin et al, 2016, supplementary material) resulted in about $9*10^5$ cm^{-3} both for nucleation event days and non-event days. Similar sulfuric acid concentrations have been reported for Finnish boreal forest measurements in autumn, where about 12% of the days were classified as nucleation event days (Kontkanen et al., 2017).

Back trajectories using HYSPLIT (http://ready.arl.noaa.gov/hypub-bin/trajtype.pl?runtype=archive; Rolph et al., 2017) were calculated using Global Data Assimilation System model data produced by the National Centers for Environmental Prediction (NCEP), and showed a clear difference in the air mass origins arriving at the measurement site for NPF and non-event days. The back trajectories were calculated as ensembles for 24 hours to arrive at 13:00 UTC (09:00 local time) on NPF days at 500m a. s. l. The back-trajectories were also calculated for each day prior to and following an NPF day. If an NPF event occurred on two consecutive days, the day after both events was used for the non-event day back-trajectory calculations. On non-NPF days, the 50th percentile of air masses originate from 2. 9°S, 58.6°W and 545 m.a.s.l., a location upstream of the Amazon river. On NPF days, the back-trajectory calculations show an origin at 2.5°S, 58.5°W and 602.5 m a. s. l.; further north, which is an area with dense rainforest. The results of the back-trajectory calculations are shown in Figure 10.

Figure 11 shows an example of an NPF event observed at the pasture site (T3) showing MAOS SMPS data, NAIS total particle concentrations, and NAIS negative ion concentrations. The intermediate ion concentrations increase during this NPF event, starting at 08:00, with a continuous growth by 10:00 to the smallest size channel of the MAOS SMPS as indicated by the blue dashed line in panel d) of Figure 11. The same can be observed in the large particle and ion (4-12 nm) channel from the NAIS (red and black lines respectively).

Table 3 shows a comparison of the median particle and ion concentrations (25th – 75th percentiles in brackets), as well as the condensation sink, for the time window 08:00-12:00 between the NPF

event and non-event days. The condensation sink was clearly lower on NPF-event days (0.0018 s^{-1}) than on non-event days (0.003 s^{-1}), and the median concentration of intermediate (2-4 nm) ions and neutral particles was 1.3 times higher on NPF- event days. The ion concentrations in the large size range were about a factor of 1.7 higher and particle concentrations in the same size range were 2.4 times higher during NPF-event times compared to non-event days.
We also compared environmental variables, including the temperature, relative humidity and wind direction. No precipitation during any of the classified NPF events themselves was observed, but on two classified NPF event days, there was precipitation before or after the NPF events (starting at 06:00 and 17:00 respectively). The median temperature and RH was about the same for NPF event and non-event days, whereas the median wind direction changed (83°N during event days and 105.5°N during non-event days), consistent with the results from the back-trajectory analysis.

Table 4 shows the calculated growth rates, particle formation rates, and condensation sinks for each classified NPF-event day. Note that here, the condensation sink is calculated for the time of the event, while in Table 2 and 3, the numbers are for the whole day. Both growth rates and particle formation quantities were determined for two different size ranges (2-3 nm and 3-7 nm), and calculated separately for the ion and particle data. The results show considerably lower ion formation rates compared with neutral particle formation rates, consistent with observations made at most other continental sites (Manninen et al., 2010; Hirsikko et al., 2011). The growth rates of particles and ions were comparable to each other and typically smaller for the 2-3 nm size range than the 3-7 nm size ranges. An increase in the particle and ion growth rate with increasing particle size has been reported previously at a few other sites (see Häkkinen et al., 2013, and references therein). We observed two regimes when looking at the neutral 3-7 nm growth rate. On 3 days, the growth rate was about 2 nmh^{-1}, with sulfuric acid concentrations of about $2*10^6$ cm^{-3}. According to theoretical calculations about 10^7 cm^{-3} of sulfuric acid molecules can account for 1 nmh^{-1} (Nieminen et al., 2010). It is most likely that other compounds are contributing to the growth. Other NPF-event days showed growth rates of about 14 nmh^{-1} for the same 3-7 nm size range, and the sulfuric acid concentration was even lower (about $6*10^5$ cm^{-3}). These growth rates are most likely driven by organic compounds (Tröstl et al., 2016). Tröstl et al. (2016) calculated that about 10^6-10^7 cm^{-3} of highly oxidized organic compounds are required to explain a growth rate of about 10 nmh^{-1}.

4 Summary and Conclusions

We performed direct measurements of atmospheric new particle formation (NPF) events in the Amazon region with state-of-the-art aerosol instrumentation. The measurement campaigns were performed at two observation sites (T0t and T3) in the vicinity of Manaus in Brazil. One site was located within the rainforest (T0t), providing long-term (September 2011 to January 2014) measurement data, to complement data from a pasture site (T3, January to October 2014).
No NPF events were observed at the T0t site during the long-term measurement period. However, we observed rain-induced ion and particle burst events ("rain-events") inside the rainforest during 264 of the 384 days. Concentrations of 2 - 4 nm and 4 - 12 nm ions and total particles were enhanced

by up to 3 orders of magnitude during such rain-events (~10^4-10^5 cm^{-3}) at T0t site. The rain-events occurred throughout the year, but the number of days with precipitation was highest from December to June corresponding to the wet season. Multiple rain-events could occur during the same day, totaling 1491 rain-events in 643 rainy days for both sites together. The duration of the rain-events ranged from a couple of minutes to 22 hours, but over 50% of the events lasted for <2 hours.

During the rain-events, 0.8 - 2 nm and 2 - 4 nm negative ions increased more than the same-size positive ions. The production of small (0.8 - 2 nm) and intermediate negative ions (2 - 4 nm) during rain-events reached a maximum of 10^5 cm^{-3} at the T0t site.

At the pasture site, we observed a clear diel pattern in the cluster ion concentration during both the wet and the dry season, with higher concentrations observed during the morning and evening. The PSM observations showed a similar diel cycle for particles >1.5 nm, with higher concentrations in the early morning, a dip in the afternoon, and an increase again in the evening after sunset. The diel cycle was less pronounced inside the rainforest, indicating that the rainforest canopy hinders vertical mixing.

We observed eight NPF events showing particle growth at the pasture site during January to March 2014. The formation rates were considerably higher for neutral particles than ions during these NPF events. The growth rates of newly-formed ions and particles were comparable to each other and showed a clear increase with increasing size in the sub-20 nm size range. We found two different regimes for growth rates in the 3-7 nm size range; 3 out of 8 NPF days had a growth rate of about 2 nmh^{-1}, and 4 out of 8 NPF days had a growth rate of about 14 nmh^{-1}. The sulfuric acid concentrations were similar for both NPF event and non-event days (approx. $9*10^5$ cm^{-3}). Most likely the observed growth for all NPF events is driven by highly oxidized organic compounds (Tröstl et al., 2016).

The back-trajectory calculations using HYSPLIT did not show any clear difference between the days with high and low growth rates. Nevertheless, there was a clear difference in air mass origin between days with NPF events, where back-trajectories originated from the rainforest, and non-event days, where back-trajectories originated from the Amazon river. As observed in SMPS measurements, particles grew to sizes of around 60 nm during all NPF events, above which they are able to act as cloud condensation nuclei (McFiggans et al, 2006; Andreae and Rosenfeld, 2008; Kerminen et al. 2012). There were clear differences in median cluster and intermediate ion concentrations between the NPF event and non-event days for the local time window of 08:00-12:00. For NPF event days, the median intermediate ion and particle concentration was higher by a factor of 1.3 compared to non-event days. The condensation sink was also lower on NPF event days (0.0016 s^{-1}) than non-event days (0.003 s^{-1}). There were no NPF events observed during the dry season, when it is likely that the condensation sink is too high for new particle formation.

Acknowledgements

We acknowledge the Academy of Finland Centre of Excellence program (grant no. 272041). We acknowledge the Atmospheric Radiation Measurement (ARM) Climate Research Facility, a user facility of the United States Department of Energy, Office of Science, sponsored by the Office of Biological and Environmental Research, and support from the Atmospheric System Research (ASR) program of that office. D.W. wishes to acknowledge the Austrian Science Fund (FWF, grant no J-3951). P Artaxo acknowledges FAPESP project 2013/05014-0 and CNPq for funding. We thank field support from Alcides Ribeiro, Bruno Takeshi and Fabio Jorge. We acknowledge logistical support from the LBA Central Office, at the INPA – Instituto Nacional de Pesquisas da Amazonia.

References

Aalto, P., Hämeri, K., Becker, E., Weber, R., Salm, J., Mäkelä, J. M., Hoell, C., O'Dowd, C. D., Karlsson, H., Hansson, H. C., Väkevä, M., Koponen, I. K., Buzorius, G., and Kulmala, M., Physical characterization of aerosol particles during nucleation events, Tellus B, 53:4, 344-358, 2001, doi: 10.1034/j.1600-0889.2001.530403.x.

Andreae, M. O.: Aerosols before pollution, Science, 315, 50–51, 2007.

Andreae, M. O., and Rosenfeld, D.: Aerosol-cloud-precipitation interactions. Part 1. The nature and sources of cloud-active aerosols, Earth-Sci. Rev., 89, 13-41, 2008, Doi: 10.1016/j.earscirev.2008.03.001.

Andreae, M. O., Acevedo, O. C., Araùjo, A., Artaxo, P., Barbosa, C. G. G., Barbosa, H. M. J., Brito, J., Carbone, S., Chi, X., Cintra, B. B. L., da Silva, N. F., Dias, N. L., Dias- Júnior, C. Q., Ditas, F., Ditz, R., Godoi, A. F. L., Godoi, R. H. M., Heimann, M., Hoffmann, T., Kesselmeier, J., Könemann, T., Krüger, M. L., Lavric, J. V., Manzi, A. O., Lopes, A. P., Martins, D. L., Mikhailov, E. F., Moran-Zuloaga, D., Nelson, B. W., Nölscher, A. C., Santos Nogueira, D., Piedade, M. T. F., Pöhlker, C., Pöschl, U., Quesada, C. A., Rizzo, L. V., Ro, C.-U., Ruckteschler, N., Sá, L. D. A., de Oliveira Sá, M., Sales, C. B., dos Santos, R. M. N., Saturno, J., Schöngart, J., Sörgel, M., de Souza, C. M., de Souza, R. A. F., Su, H., Targhetta, N., Tóta, J., Trebs, I., Trumbore, S., van Eijck, A., Walter, D., Wang, Z., Weber, B., Williams, J., Winderlich, J., Wittmann, F., Wolff, S., and Yáñez-Serrano, A. M.: The Amazon Tall Tower Observatory (ATTO): overview of pilot measurements on ecosystem ecology, meteorology, trace gases, and aerosols, Atmos. Chem. Phys., 15, 10723–10776, 2015, doi:10.5194/acp-15- 10723-2015.

Artaxo, P., Rizzo, L. V., Brito, J. F., Barbosa, H. M. J., Arana, A., Sena, E. T., Cirino, G. G., Bastos, W., Martin, S. T., and Andreae, M. O.: Atmospheric aerosols in Amazonia and land use change: from natural biogenic to biomass burning conditions, Faraday Discuss., 165, 203–235, 2013.

Asmi, E., Sipilä, M., Manninen, H. E., Vanhanen, J., Lehtipalo, K., Gagné, S., Neitola, K., Mirme, A., Mirme, S., Tamm, E., Uin, J., Komsaare, K., Attoui, M., and Kulmala, M.: Results of the first air ion spectrometer calibration and intercomparison workshop, Atmos. Chem. Phys., 9, 141-154, 2009, doi:10.5194/acp-9-141-2009.

Backman, J., Rizzo, L. V., Hakala, J., Nieminen, T., Manninen, H. E., Morais, F., Aalto, P. P., Siivola, E., Carbone, S., Hillamo, R., Artaxo, P., Virkkula, A., Petäjä, T., and Kulmala, M.: On the diurnal cycle of urban aerosols, black carbon and the occurrence of new particle formation events in springtime São Paulo, Brazil, Atmos. Chem. Phys., 12, 11733-11751, 2012, doi:10.5194/acp-12-11733-2012.

Dunne, E., Gordon, H., Kürten, A., Almeida, J., Duplissy, J., Williamson, C., Ortega, I. K., Pringle, J.K., Adamov, A., Baltensperger, U., Barmet, P., Benduhn, F., Bianchi, F., Breitenlechner, M., Clarke, A., Curtius, J., Dommen, J., Donahue, N. M., Ehrhart, S., Flagan, R. C.,Franchin, A., Guida, R., Hakala, J., Hansel, A., Heinritzi, M., Jokinen, T., Kangasluoma, J., Kirkby, J., Kulmala, M., Kupc, A., Lawler, M. J., Lehtipalo, K., Makhmutov, V., Mann, G., Mathot, S., Merikanto, J., Miettinen, P., Nenes, A., Onnela, A., Rap, A., Reddington, C. L. S., Riccobono, F., Richards, N. D. A.,Rissanen, M. P., Rondo, L., Sarnela, N., Schobesberger, S., Sengupta, K., Simon, M., Sipilä, M., Smith, J. N., Stozkhov, Y., Tomé, A., Tröstl, J., Wagner, P. E., Wimmer, D., Winkler, P. M., Worsnop, D. R., and Carslaw K. S., Global atmospheric particle formation from CERN CLOUD measurements, Science, 354: 6316, 2016.

Dos Santos, V. N., Herrmann, E., Manninen, H. E., Hussein, T., Hakala, J., Nieminen, T., Aalto, P. P., Merkel, M., Wiedensohler, A., Kulmala, M., Petäjä, T., and Hämeri, K., Atmos. Chem. Phys., 15; 23:13717-13737, 2015, doi: 10.5194/acp-15-13717-2015.

Häkkinen, S. A. K., Manninen, H. E., Yli-Juuti, T., Merikanto, J., Kajos, M. K., Nieminen, T., D'Andrea, S. D., Asmi, A., Pierce, J. R., Kulmala, M. and Riipinen, I.: Semi-empirical parameterization of size-dependent atmospheric nanoparticle growth in continental environments, Atmos. Chem. Phys., 13, 15: 7665-7682, 2013, doi: 10.5194/acp-13-7665-2013.

Harrison, R. G., and Carslaw, K. S., Ion-Aerosol-cloud processes in the lower atmosphere, Rev. Geophys., 41, 3 / 1012, 2003, doi:10.1029/2002RG000114.

Hirsikko, A, Laakso, L, Horrak, U, Aalto, P. P., Kerminen, V.-M., and Kulmala, M., Annual and size dependent variation of growth rates and ion concentrations in boreal forest, Bor. Environ. Res., 10, 357-369, 2005.

Hirsikko, A., Bergman, T., Laakso, L., Dal Maso, M., Riipinen, I., Hõrrak, U., and Kulmala, M., Identification and classification of the formation of intermediate ions measured in boreal forest, Atmos. Chem. Phys., 7, 201-210, 2007.

Hirsikko, A., Nieminen, T., Gagné, S., Lehtipalo, K., Manninen, H. E., Ehn, M., Hõrrak, U. Kerminen, V-M., Laakso, L., McMurry, P. H., Mirme, A., Mirme, S., Petäjä, T., Tammet, H., Vakkari, V., Vana, M., and Kulmala, M. Atmospheric ions and nucleation: a review of observations, Atmos. Chem. Phys., 11, 767-798, 2011, doi: 10.5194/acp-11-767-2011.

Hoppel, W. A., Theory of the electrode effect, J. Atmos. Terr. Phys., Vol. 22, 1967.

Hõrrak, U., Salm, J., and Tammet, H., Bursts of intermediate ions in atmospheric air, J. Geophys. Res.: Atmos., 103: 13909-13915, 1998, doi: 10.1029/97JD01570.

Hõrrak, U., Tammet, H., Aalto, P. P., Vana, M., Hirsikko, A., Laakso, L., and Kulmala, M.: Formation of charged particles associated with rainfall: atmospheric measurements and lab experiments, Rep. Ser. Aerosol Sci., 80, 180–185, 2006.

Kalivitis, N., Stavroulas, I., Bougiatioti, A., Kouvarakis, G., Gagné, S., Manninen, H. E., Kulmala, M., and Mihalopoulos, N.: Night-time enhanced atmospheric ion concentrations in the marine boundary layer, Atmos. Chem. Phys., 12, 3627-3638, 2012, doi:10.5194/acp-12-3627-2012.

Kangasluoma J., Kuang C., Wimmer D., Rissanen M. P., Lehtipalo K., Ehn M., Worsnop, D. R., Wang, J., Kulmala M., and Petäjä T., Sub-3nm particle size and composition dependent response of a nano-CPC battery, Atmos. Meas. Tech., 7, 689–700, 2014, doi:10.5194/amt-7-689-2014.

Kerminen, V-M, Paramonov, M., Anttila, T., Riipinen, I., Fountoukis, C, Korhonen, H., Asmi, E., Laakso, L., Lihäväinen, H., Swietlicki, E., Svenningsson, B., Asmi, A., Pandis, S. N, Kulmala, M., and Petäjä, T., Cloud condensation nuclei production associated with atmospheric nucleation: a synthesis based on existing literature and new results, Atmos. Chem. Phys., 12, 24: 12037-12059, 2012, doi: 10.5194/acp-12-12037-2012.

Kontkanen, J., Lehtipalo, K., Ahonen, L., Kangasluoma, J., Manninen, H. E., Hakala, J., Rose, C., Sellegri, K., Xiao, S., Wang, L., Qi, X., Nie, W., Ding, A., Yu, H., Lee, S., Kerminen, V.-M., Petäjä, T.., and Kulmala, M., Measurements of sub-3 nm particles using a particle size magnifier in different environments: from clean mountain top to polluted megacities, Atmos. Chem. Phys., 2163–2187, 2017, doi:10.5194/acp-17-2163-2017.

Kulmala, M., Vehkämäki, H, Petäjä, T., Dal Maso, M., Lauri, A, Kerminen, VM, Birmili, and McMurry, PH., Formation and growth rates of ultrafine atmospheric particles: a review of observations, J. Aerosol Sci., 35,143-176, 2004.

Kulmala, M., Petäjä, T., Nieminen, T., Sipilä, M., Manninen, H. E., Lehtipalo, K., Dal Maso, M., Aalto, P. P., Junninen, H., Paasonen, P., Riipinen, I., Lehtinen, K. E. J., Laaksonen, A., and Kerminen, V.-M.: Measurement of the nucleation of atmospheric aerosol particles, Nat. Protoc., 7, 1651–1667, 2012.

Kulmala, M., Kontkanen, J., Junninen, H., Lehtipalo, K., Manninen, HE, Nieminen, T., Petäjä, T., Sipilä, M., Schobesberger, S., Rantala, P., Franchin, A, Jokinen, T., Järvinen, E., Äijala, M., Kangasluoma, J., Hakala, J., Aalto, P. P., Paasonen, P., Mikkilä, J., Vanhanen, J., Aalto, J., Hakola,

Deleted: ¶

H., Makkonen, U., Ruuskanen, T., Mauldin, R. L., III, Duplissy, J., Vehkämäki, H., Back, J., Kortelainen, A., Riipinen, I., Kurten, T., Johnston, M. V., Smith, J. N. Ehn, M., Mentel, T. F., Lehtinen, K. E. J., Laaksonen, A., Kerminen, V.-M., and Worsnop, D. R., Direct Observations of Atmospheric Aerosol Nucleation, Science, 339, 943, 2013.

Kulmala, M., Petäjä, T. Ehn, M., Thornton, J., Sipilä, M., Worsnop, D. R., and Kerminen, V. -M., Chemistry of Atmospheric Nucleation: On the Recent Advances on Precursor Characterization and Atmospheric Cluster Composition in Connection with Atmospheric New Particle Formation, Annu. Rev. Phys. Chem., 65, 21–37, 2014.

Kulmala, M., Luoma, K., Virkkula, A, Petäjä, T., Paasonen, P., Kerminen, V.-M. Nie, W., Qi, X., Shen, Y., Chi, X., and Ding, A., On the mode-segregated aerosol particle number concentration load: contributions of primary and secondary particles in Hyytiala and Nanjing Bor. Environ. Res., 21, 319-331, 2016.

Leino, K., Nieminen, T., Manninen, H. E., Petäjä, T., Kerminen, V.-M., and Kulmala, M., Intermediate ions as a strong indicator of new particle formation bursts in a boreal forest, Bor. Environ. Res., 21, 274-286, 2016.

Lelieveld J., Butler, T. M., Crowley, J. N., Dillon, T. J., Fischer, H., Ganzeveld, L., Harder, H., Lawrence, M. G., Martinez, M., Taraborrelli, D., and Williams, J., Atmospheric oxidation capacity sustained by a tropical forest, Nature 452, 737-740, 2008.

Manninen, H. E., Nieminen, T., Asmi, E., Gagné, S., Häkkinen, S., Lehtipalo, K., Aalto, P., Vana, M., Mirme, A., Mirme, S., Hõrrak, U., Plass-Dülmer, C., Stange, G., Kiss, G., Hoffer, A., Törő, N., Moerman, M., Henzing, B., de Leeuw, G., Brinkenberg, M., Kouvarakis, G. N., Bougiatioti, A., Mihalopoulos, N., O'Dowd, C., Ceburnis, D., Arneth, A., Svenningsson, B., Swietlicki, E., Tarozzi, L., Decesari, S., Facchini, M. C., Birmili, W., Sonntag, A., Wiedensohler, A., Boulon, J., Sellegri, K., Laj, P., Gysel, M., Bukowiecki, N., Weingartner, E., Wehrle, G., Laaksonen, A., Hamed, A., Joutsensaari, J., Petäjä, T., Kerminen, V.-M., and Kulmala, M.: EUCAARI ion spectrometer measurements at 12 European sites – analysis of new particle formation events, Atmos. Chem. Phys., 10, 7907-7927, 2010, doi:10.5194/acp-10-7907-2010.

Manninen, H. E., Mirme, S., Mirme, A., Petäjä, T., and Kulmala, M.: How to reliably detect molecular clusters and nucleation mode particles with Neutral cluster and Air Ion Spectrometer (NAIS), Atmos. Meas. Tech., 9, 3577-3605, 2016, doi:10.5194/amt-9-3577-2016.

Martin, S. T., Andreae, M. O., Artaxo, P., Baumgardner, D., Chen, Q., Goldstein, A. H., Guenther, A., Heald, C. L., Mayol-Bracero, O. L., McMurry, P. H., Pauliquevis, T., Poeschl, U., Prather, K. A., Roberts, G. C., Saleska, S. R., Silva Dias, M. A., Spracklen, D. V., Swietlicki, E., and Trebs, I., Sources and properties of Amazonian aerosol particles, Rev. Geophys., 48, RG2002, 2010a, doi: 10.1029/2008RG000280.

Martin, S. T., Andreae, M. O., Althausen, D., Artaxo, P., Baars, H., Borrmann, S., Chen, Q., Farmer, D. K., Guenther, A., Gunther, S. S., Jimenez, J. L., Karl, T., Longo, K., Manzi, A., Müller, T., Pauliquevis, T., Petters, M. D., Prenni, A. J., Pöschl, U., Rizzo, L. V., Schneider, J., Smith, J. N., Swietlicki, E., Tota, J., Wang, J., Wiedensohler, A., and Zorn, S. R.: An overview of the Amazonian Aerosol Characterization Experiment 2008 (AMAZE-08), Atmos. Chem. Phys., 10, 11415–11438, 2010b, doi:10.5194/acp-10-11415-2010.

Martin, S. T., Artaxo, P., Machado, L. A. T., Manzi, A. O., Souza, R. A. F., Schumacher, C., Wang, J., Andreae, M. O., Barbosa, H. M. J., Fan, J., Fisch, G., Goldstein, A. H., Guenther, A., Jimenez, J. L., Pöschl, U., Silva Dias, M. A., Smith, J. N., and Wendisch, M.: Introduction: Observations and Modeling of the Green Ocean Amazon (GoAmazon2014/5), Atmos. Chem. Phys., 16, 4785-4797, 2016, doi:10.5194/acp-16-4785-2016.

Martin, S. T., Artaxo P., Machado, L., Manzi, A. O., Souza, R. A. F., Schumacher, C., Wang, J., Biscaro, T., Brito, J., Calheiros, A., Jardine, K., Medeiros, A., Portela, B., de Sá, S. S., Adachi, K., Aiken, A. C., Albrecht, R., Alexander, L., Andreae, M. O., Barbosa, H. M. J., Buseck, P., Chand, D., Comstock, J. M., Day, D. A., Dubey, M., Fan, J., Fast, J., Fisch, G., Fortner, E., Giangrande, S., Gilles, M., Goldstein, A. H., Guenther, A., Hubbe, J., Jensen, M., Jimenez, J. L., Keutsch, F. N., Kim, S., Kuang, C., Laskin, A., McKinney, K., Mei, F., Miller, M., Nascimento, R., Pauliquevis, T., Pekour, M., Peres, J., Petäjä, T, Pöhlker, C., Pöschl, U., Rizzo, L., Schmid, B., Shilling, J. E., Silva Dias, M. A., Smith, J. N., Tomlinson, J. M., Tóta, J., and Wendisch, M., The Green Ocean Amazon Experiment (GoAmazon2014/5) observes pollution affecting gases, aerosols, clouds and rainfall over the rain forest, Bull. Am. Meteor. Soc., 2017, doi:10.1175/BAMS-D-15-00221.1.

Mather, J. H., and Voyles, J. W.: The ARM Climate Research Facility: A review of structure and capabilities, Bull. Am. Meteor. Soc., 94, 377–392, 2013.

McFiggans, G, Artaxo, P., Baltensperger, U., Coe, H., Facchini, M. C., Feingold, G., Fuzzi, S., Gysel, M., Laaksonen, A., Lohmann, U., Mentel, T. F., Murphy, D. M., O'Dowd, C. D., Snider, J. R.) and Weingartner, E., The effect of physical and chemical aerosol properties on warm cloud droplet activation, Atmos. Chem. Phys, 6, 2593-2649, 2006.

Merikanto, J., Spracklen, D. V., Mann, G. W., Pickering, S. J., and Carslaw, K. S.: Impact of nucleation on global CCN, Atmos. Chem. Phys., 9, 8601-8616, 2009, doi:10.5194/acp-9-8601-2009.

Nieminen, T., Yli-Juuti, T., Manninen, H. E., Petäjä, T., Kerminen, V.-M., and Kulmala, M.: Technical note: New particle formation event forecasts during PEGASOS–Zeppelin Northern mission 2013 in Hyytiälä, Finland, Atmos. Chem. Phys., 15, 12385-12396, 2015, doi:10.5194/acp-15-12385-2015.

Nieminen, T., Lehtinen, K. E. J., and Kulmala, M., Sub-10 nm particle growth by vapor condensation - effects of vapor molecule size and particle thermal speed, Atmos. Chem. Phys., 10, 9773-9779, 2010, DOI: 10.5194/acp-10-9773-2010.

Rose, C., Sellegri, K., Velarde, F., Moreno, I., Ramonet, M., Weinhold, K., Krejci, R. Ginot, P., Andrade, M., Wiedensohler, A., and Laj, P., Frequent nucleation events at the high altitude station of

Chacaltaya (5240 m a.s.l.), Bolivia, Atmos. Environ., 102, 18-29, DOI: 10.1016/j.atmosenv.2014.11.015, 2015.

Rolph, G., A. Stein and B. Stunder, Real-time Environmental Applications and Display sYstem: READY, Environmental Modelling & Software, 95, 210-228, 2017, doi:10.1016/j.envsoft.2017.06.025.

Tammet, H., Hõrrak, U., and Kulmala, M.: Negatively charged nanoparticles produced by splashing of water, Atmos. Chem. Phys., 9, 357-367, 2009, doi:10.5194/acp-9-357-2009.

Tröstl, J., Chuang, W. K., Gordon, H., Heinritzi, M., Yan, C., Molteni, U., Ahlm, L., Frege, C., Bianchi, F., Wagner, R., Simon, M., Lehtipalo, K., Williamson, C., Craven, J. S., Duplissy, J., Adamov, A., Almeida, J., Bernhammer, A.-K., Breitenlechner, M., Brilke, S., Dias, A., Ehrhart, S., Flagan, R. C., Franchin, A., Fuchs, C., Guida, R., Gysel, M., Hansel, A., Hoyle, C. R., Jokinen, T., Junninen, H., Kangasluoma, J., Keskinen, H., Kim, J., Krapf, M., Kürten, A., Laaksonen, A., Lawler, M.,Leiminger, M., Mathot, S., Möhler, O., Nieminen, T., Onnela, A., Petäjä, T., Piel, F. – M., Miettinen, P., Rissanen, M. P., Rondo, L., Sarnela, N., Schobesberger, S., Sengupta, K., Sipilä, M., Smith, J. N., Steiner, G., Tomè, A., Virtanen, A., Wagner, A.C., Weingartner, E., Wimmer, D., Winkler, P. M., Ye, P., Carslaw, K. S., Curtius, J., Dommen, J., Kirkby, J., Kulmala, M., Riipinen, I., Worsnop, D.R., Donahue, N. M. and Baltensperger, U., The role of low-volatility organic compounds in initial particle growth in the atmosphere, Nature, 533, 527-531, 2016, doi:10.1038/nature18271.

Vanhanen, J., Mikkilä, J., Lehtipalo, K., Sipilä, M., Manninen, H. E., Siivola, E., Petäjä, T., and Kulmala, M.: Particle size magnifier for nano-CN detection. Aerosol Sci. Technol., 45:533–542, 2011.

Suni, T., Kulmala, M., Hirsikko, A., Bergman, T., Laakso, L., Aalto, P. P., Leuning, R., Cleugh, H., Zegelin, S., Hughes, D., van Gorsel, E., Kitchen, M., Vana, M., Hõrrak, U., Mirme, S., Mirme, A., Sevanto, S., Twining, J., and Tadros, C.: Formation and characteristics of ions and charged aerosol particles in a native Australian Eucalypt forest, Atmos. Chem. Phys., 8, 129-139, 2008, doi:10.5194/acp-8-129-2008.

Svenningsson, B., Arneth, A., Hayward, S., Holst, T., Massling, A., Swietlicki, E., Hirsikko, A., Junninen, H., Riipinen, I., Vana, M., Dal Maso, M., Hussein, T., and Kulmala, M.: Aerosol particle formation events and analysis of high growth rates observed above a subarctic wetland-forest mosaic, TellusB, 60B, 353–364, 2008.

Vana, M., Kulmala, M., Dal Maso, M. and Hõrrak, U., Comparative study of nucleation mode aerosol particles and intermediate air ions formation events at three sites, J. Geophys. Res., VOL. 109, D17201, 2004, doi:10.1029/2003JD004413.

Vana, M., Ehn, M., Petäjä, T., Vuollekoski, H., Aalto, P., de Leeuw, G., Ceburnis, D., O'Dowd, C. D., and Kulmala, M.Characteristic features of air ions at Mace Head on the west coast of Ireland, Atmos. Res., 90, 278-286, 2008, DOI: 10.1016/j.atmosres.2008.04.007.

Vanhanen, J., Mikkilä, J., Lehtipalo, K., Sipilä, M., Manninen, H. E., Siivola, E., Petäjä, T. and Kulmala, M. (2011), Particle Size Magnifier for Nano-CN Detection, Aerosol Sci. Technol., 45: 4, 533 — 542, 2011, DOI: 10.1080/02786826.2010.547889.

Wagner, R., Manninen, H. E., Franchin, A., Lehtipalo, K., Mirme, S., Steiner, G., Petäjä, T., and Kulmala, M.: On the accuracy of ion measurements using a Neutral cluster and Air Ion Spectrometer, Bor. Environ. Res., 21, 230-241, 2016.

Wang, J., Krejci, R., Giangrande, S., Kuang, C., Barbosa, H. M. J., Brito, J., Carbone, S., Chi, X., Comstock, J., Ditas, F., Lavric, J., Manninen, H. E., Mei, F., Moran-Zuloaga, D., Pöhlker, C., Pöhlker, M. L., Saturno, J., Schmid, B., Souza, R. A. F., Springston, S. R., Tomlinson, J. M., Toto, T., Walter, D., Wimmer, D., Smith, J. N., Kulmala, M., Machado, L.A. T., Artaxo, P., Andreae, M. O., Petäjä, T., and Martin, S. T., Amazon boundary layer aerosol concentration sustained by vertical transport during rainfall, Nature, 2016, doi:10.1038/nature19819.

Wang, M., and Penner, J. E., Aerosol indirect forcing in a global model with particle nucleation, Atmos. Chem. Phys., 9:1, 239-260, 2009.

Yu, F., and Luo, G.: Simulation of particle size distribution with a global aerosol model: contribution of nucleation to aerosol and CCN number concentrations, Atmos. Chem. Phys., 9: 20, 7691-7710, 2009.

Zhou, J., Swietlicki, E., Hansson, H. C. and Artaxo, P.: Submicrometer aerosol particle size distribution and hygroscopic growth measured in the Amazon rain forest during the wet season, J. Geophys. Res. D Atmos., 107(20), doi:10.1029/2000JD000203, 2002.

Tables

Table 1. Overall data availability for the measurements presented in the manuscript.

		# of days with rain data	# of days with rain event	NAIS particle data	NAIS ion data	NPF
2011	August	5	2	0	0	0
	September	6	1	4	4	0
	October	28	14	31	31	0
	November	30	18	30	30	0
	December	31	23	16	16	0
total 2011		**100**	**58**	**81**	**81**	**0**
2012	January	31	31	31	31	0
	February	29	18	29	29	0
	March	31	0	9	9	0
	April	30	29	29	29	0
	May	31	25	16	16	0
	June	30	23	4	4	0
	July	31	24	0	0	0
	August	31	12	0	0	0
	September	30	4	0	0	0
	October	31	0	0	0	0
	November	30	5	0	0	0
	December	31	24	16	16	0
total 2012		**366**	**195**	**134**	**134**	**0**
2013	January	31	26	31	31	0
	February	28	28	28	28	0
	March	31	24	31	31	0
	April	30	29	30	30	0
	May	31	27	31	31	0
	June	30	23	30	30	0
	July	31	9	31	31	0
	August	31	15	26	26	0
	September	30	13	30	30	0
	October	30	16	31	31	0
	November	30	24	30	30	0
	December	31	17	31	31	0
total 2013		**364**	**251**	**360**	**360**	**0**
2014	January T0t (rain data only from T0t)	20	13	25	25	0
	January T3	0	0	5	5	2
	February	28	23	28	28	2
	March	31	28	31	31	4
	April	30	27	23	23	0
	May	0	0	0	0	0
	June	0	0	0	0	0
	July	0	0	0	0	0

		# of days with rain data	# of days with rain event	NAIS particle data	NAIS ion data	NPF
	August	31	13	6	6	0
	September	30	16	30	12	0
	October	31	19	13	13	0
total 2014		**201**	**139**	**161**	**143**	**8**
total		**1031**	**643**	**736**	**718**	**8**

Table 2. A comparison of the two measurement sites and the wet and the dry season. The values from the pasture site are on the left-hand side, the values from the inside the rainforest site on the right- hand side. The months for the wet season are January to June and July to December for both measurement sites. Aerosol and ion parameters from the NAIS measurements listed are: the ion concentrations in three size bins (0.8-2, 2 - 4 and 4 - 12 nm); the neutral particle concentrations in two different size bins from the NAIS (2 - 4 and 4 -12 nm), and the total particle concentrations (>10 nm) from the MAO CPC measurements and the calculated condensation sink values from the SMPS are also shown. The numbers present median values and the 25th-75th percentiles are in the brackets. The environmental parameters shown are the temperature, the relative humidity, the precipitation rate, the wind direction and the wind speed.

	Pasture site (T3)		Inside rainforest (T0t)	
Particle and ion concentrations				
Season	*Wet*	*Dry*	*Wet*	*Dry*
Cluster ions (0.8-2 nm) [cm^{-3}]	1800)	890(-) (468-1400)	856 (-) (535 -1300) 549(+) (298 - 924)	952(-) (637-1400) 537 (+) (297-915)
Intermediate ions (2-4 nm) [cm^{-3}]	6 (-) (4-11)	5(-) (1-10)	17(-) (10-28) 34(+) (20-48)	17 (-) (10-28) 34(+) (21-48)
Large ions (4-12 nm) [cm^{-3}]	20(-) (11-32)	12(-) (4 - 25)	8(-) (4-16) 8(+) (4-14)	8(-) (4-16) 8 (4-14)
Intermediate particles (2-4 nm) [cm^{-3}]	612 (304 - 1000)	640 (291 - 1200)	358 (128-713)	404 (155-819)
Large particles (4 - 12 nm) [cm^{-3}]	363 (196 - 675)	314 (179 - 551)	115 (42-250)	141(-) (52-313)
CPC total particles (>10 nm) [cm^{-3}]	928 (516 - 1500)	2000 (1100 - 3000)	-	-
SMPS condensation sink [s^{-1}]	1.9 e-3 (9.5e-4-2.4e-3)	5.2 e-3 (2.3e-3-6.1e-3)	-	-
Environmental parameters				
Temp [°C]	26 (24.4 – 29.9)	25.9 (24.5 – 28.6)	24.1 (23.2 -25.6)	24.5 (23.4 - 26.5)
RH [%]	92.8 (76 – 97.3)	94.6 (83 - 98)	96.9 (93-98)	94.4 (87 - 97)
Total average precipitation [mm]	35.6	49	578	236
Wind direction [°; relative to north]	114.7 (32.7 – 231.5)	94.7 (45.8 – 178.6)	94 (58-138)	105 (58 - 167)
Wind speed [m s^{-1}]	1.1 (0.5 – 2.1)	1.3 (0.6 – 2.4)	0.2 (0.2 – 0.3)	0.2 (0.2 – 0.3)

Table 3. The parameters from the pasture site for NPF days and non-event days are shown. The values shown are: the median total particle concentration measured by a CPC, the median neutral particle concentrations measured by the NAIS in two size ranges (2 - 4 and 4 - 12 nm), and the median negative ion concentrations from the NAIS in three size ranges (0.8-2, 2 - 4 and 4 – 12 nm). The values are calculated for the time window 08:00 – 12:00, which is when the NPF events take place. The numbers in the brackets represent the 25th and 75th percentiles. The second part of the table includes median numbers of environmental parameters for the whole day: temperature, RH, Precipitation and wind direction for NPF /non-event days.

Particle and ion concentrations- 08:00 – 12:00 LT		
	NPF day	**Non NPF day**
Cluster ions (0.8-2 nm) [cm^{-3}]	1000 (-) (862 - 1300)	1000 (-) (865 - 1300)
Intermediate ions (2-4 nm) [cm^{-3}]	10 (-) (5 - 22)	8 (-) (4-15)
Large ions (4-12 nm) [cm^{-3}]	29 (-) (17 - 56)	17 (-) (7 - 33)
Intermediate particles (2-4 nm) [cm^{-3}]	800 (865 - 1300)	640 (281 - 1200)
Large particles (4-12 nm) [cm^{-3}]	785 (446-1300)	321 (170 - 580)
CPC total particles (>10 nm) [cm^{-3}]	1000 (607 - 1900)	938 (400 - 1800)
Full day data		
SMPS Condensation sink [s^{-1}]	1.8e-3 (1e-3-2.8e-3)	3.2e-3 (1.7e-3-5.3e-3)
Environmental parameters-full day		
	NPF day	**Non NPF day**
Temp [°C]	26.5 (24.8 – 31.9)	26 (24.4 – 29.2)
RH [%]	90.6 (66.6 –96.3)	93.5 (78.9 – 97.6)
Precipitation rate [mm hr^{-1}]	0.16 (0.15 – 0.35)	0 (0 – 0.16)
Wind direction [°; relative to north]	83.8 (7.3 – 200.6)	104.2 (39.6 – 215.5)
Wind speed [m s^{-1}]	0.9 (0.23 – 1.8)	1.25 (0.6 – 2.3)

Table 4. The growth rates (GR, nmh^{-1}) and the nucleation rates (J; cm^{-3}s^{-1}) determined from the NAIS ion and particle data for each nucleation event are presented. Both, the GR values and the nucleation rates present median values for positive and negative ions. Also, the median values for the calculated condensation sink values (CS; s^{-1}) for each event are shown. The condensation sink parameter is calculated from the SMPS size distributions. The last line of the table shows the median values for GR and J for all the nucleation event days are shown, except the ion GR at 2-3 nm of 19.8 nmh^{-1} on 06.02.2014 is considered to be an outlier and not included in the median.

Size bins	**2-3 nm**				**3-7 nm**				
	Particles		*ions*		*Particles*		*Ions*		
	GR (nm h^{-1})	**J** (cm^{-3}s^{-1})	**GR** (nm h^{-1})	**J** (cm^{-3}s^{-1})	**GR** (nm h^{-1})	**J** (cm^{-3}s^{-1})	**GR** (nm h^{-1})	**J** (cm^{-3}s^{-1})	**CS** (s^{-1})
29.01.2014	0.8	0.19	1.4	0.003	2.8	0.097	1.7	0.001	-
30.01.2014	-	-	3.7	0.011	13.6	-	7.1	0.13	0.00076
06.02.2014	0.8	-	19.8	0.07	29	0.87	11	0.01	0.0016
12.02.2014	0.7	0.17	1.2	0.005	1.3	0.09	1.2	0.003	0.0016
12.03.2014	1.1	0.2	1.7	0.002	13.3	-	11.2	0.008	0.0014
13.03.2014	1.5	0.2	1.6	-	1.2	-	8	-	0.0015
18.03.2014	-	-	0.7	0.002	-	-	7.7	0.009	0.0017
25.03.2014	0.8	0.11	-	-	15.7	0.4	15.8	0.018	0.0017
median	0.8	0.18	1.6	0.004	13.3	0.25	7.85	0.009	0.0016

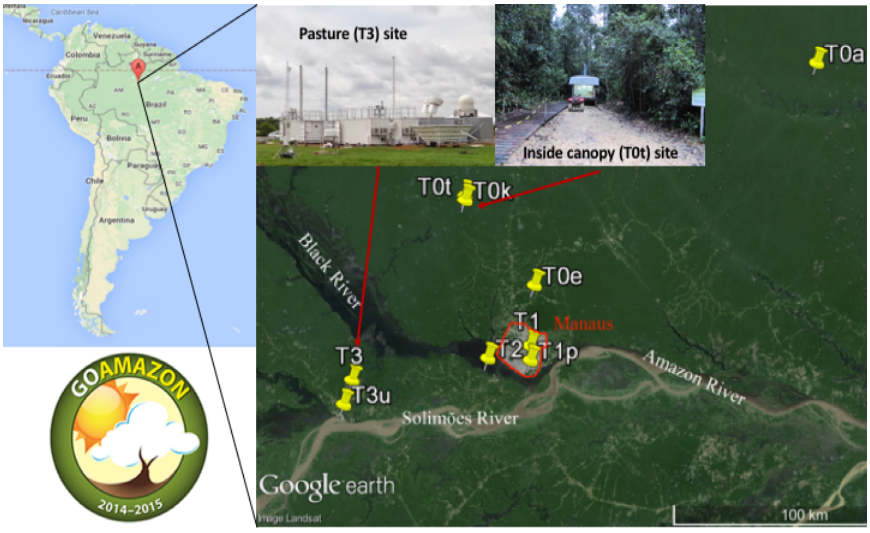

Figure 1. Location on the map and photos of the inside rainforest (T0t) and open pasture (T3) sampling sites in Amazonas. The left column shows a map of South America and the right side shows a satellite view and photos of the T0t and T3 environment.

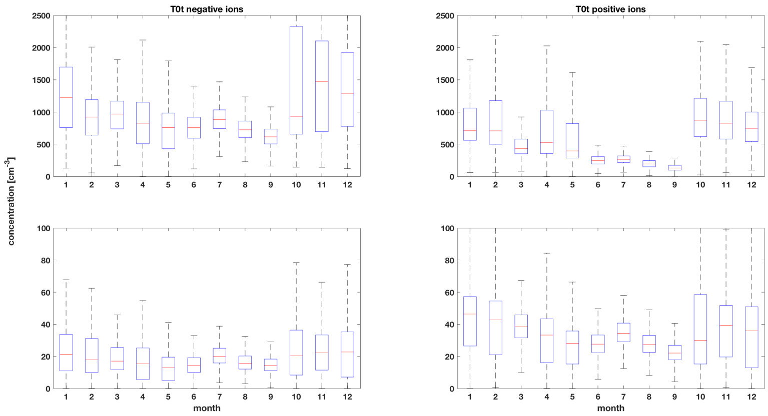

Figure 2: The median annual variations for positive and negative cluster (0.8 – 2nm) and intermediate (2 - 4 nm) ions, from the inside the rainforest site are shown. The boxes show the 25th-75th percentile and the whiskers are 1.5 x IQR (interquartile range), data points beyond the whiskers are considered outliers.

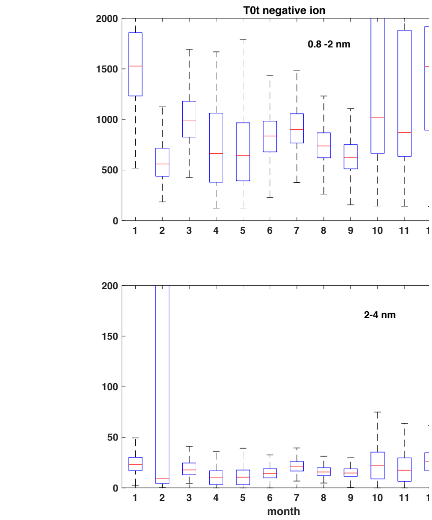

Deleted:

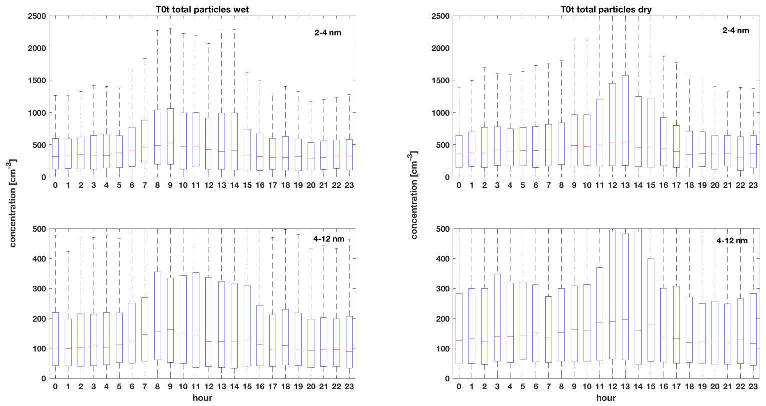

Figure 3. The median diel patterns of the intermediate (2-4 nm) and the large (4-12 nm) particles from the NAIS measurements at the T0t measurement site are shown. On the left -hand side are the values for the wet and on the right-hand side the values for the dry season. The boxes represent 25th – 75th percentiles and the whiskers are 1.5 x IQR (interquartile range), data points beyond the whiskers are considered outliers.

Deleted: *<object><object>*

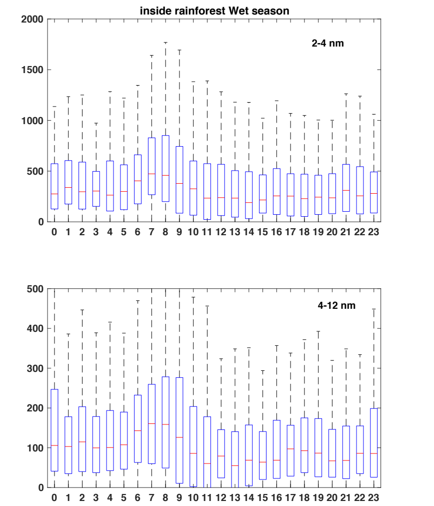

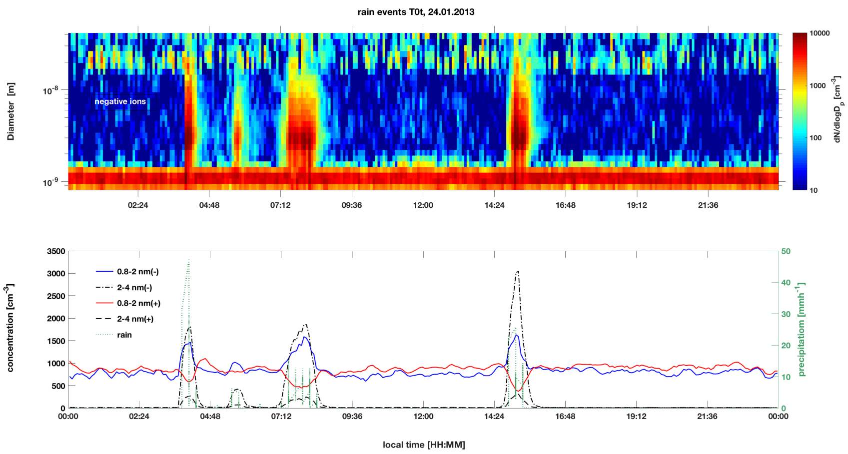

Figure 4. An example for a rain event at the T0t, inside the rainforest measurement site is shown. The upper panel shows the surface Figure of the NAIS negative ion channel. The lower panel shows (i) the concentrations of positive (red line), (ii) negative (blue line) cluster ions (0.8 – 2 nm), (iv) positive (dashed black line), and (v) negative (dot-dashed line) intermediate (2 -4 nm) ions on the left - hand axis. The precipitation rate in mmh^{-1} is shown in green on the right - hand axis.

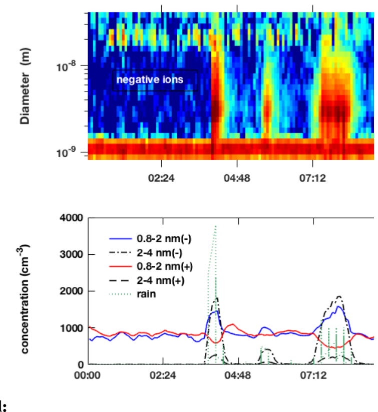

Deleted:

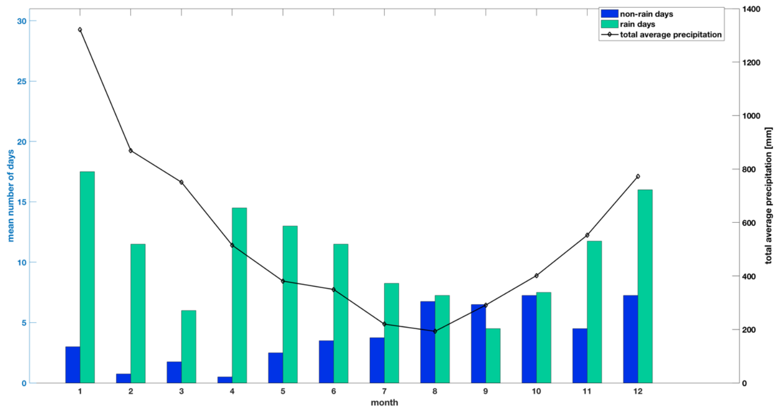

Figure 5. The statistics of the precipitation days at the T0t site are shown. The blue bars show the mean number of days per month with no precipitation and the green bars the mean number of days per month with precipitation rates above zero. The black line shows the average total precipitation per month in mm on the right-hand axis.

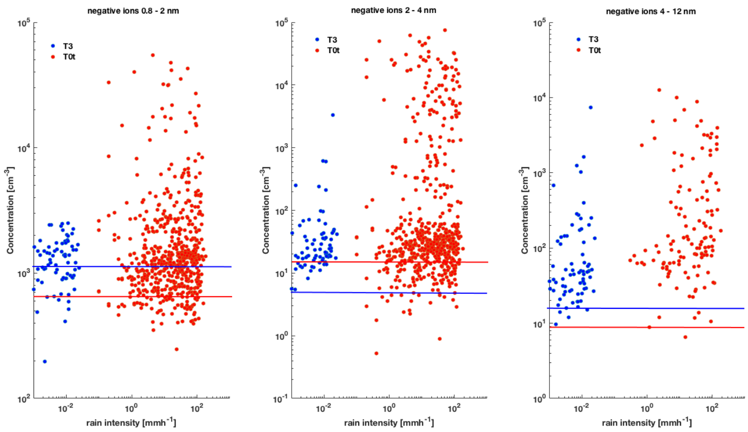

Figure 6. The maximum (99 percentile) negative ion concentrations as a function of rain intensity at the inside rainforest site (T0t) between September 2011 and January 2014 (red circles) are shown. For comparison, the ion concentrations from the open pasture site are added (blue circles). The lines indicate the median ion concentrations at the absence of precipitation for T0t (red) and T3 (blue).

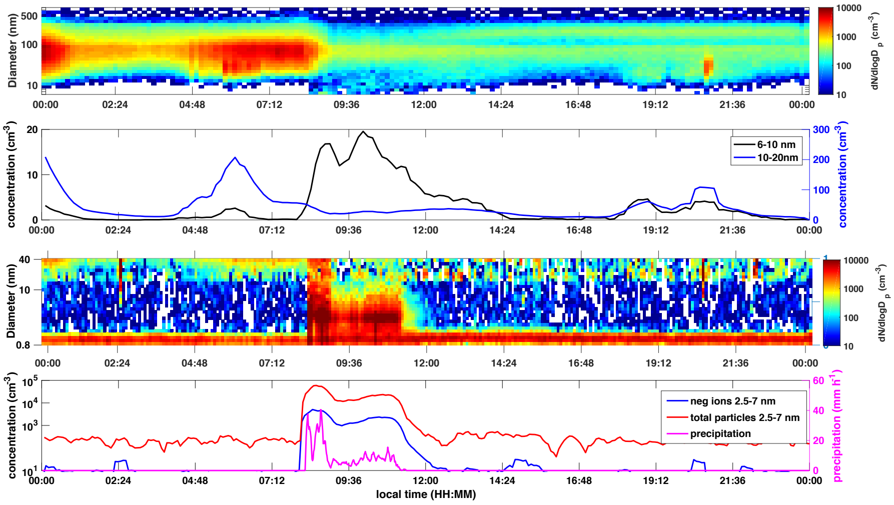

Figure 7. An Example for of a rain-induced event is shown. The upper panel shows the surface Figure for total particles (DMPS). The second panel from the top shows the particle concentrations measured by the DMPS for the size range of 6-10 nm (black line, left-hand axis) and the size range of 10-20 nm (blue line, right-hand axis). The third panel from the top shows the surface Figure for the negative ions, measured by the NAIS. The lower panel shows the negative ion concentrations for 2.5-7 nm in blue and the neutral particle concentration in the same size range from the NAIS in red. For the neutral particles, the scale is on the left-hand axis. The pink trace shows the precipitation rate in mm h^{-1} on the right-hand axis.

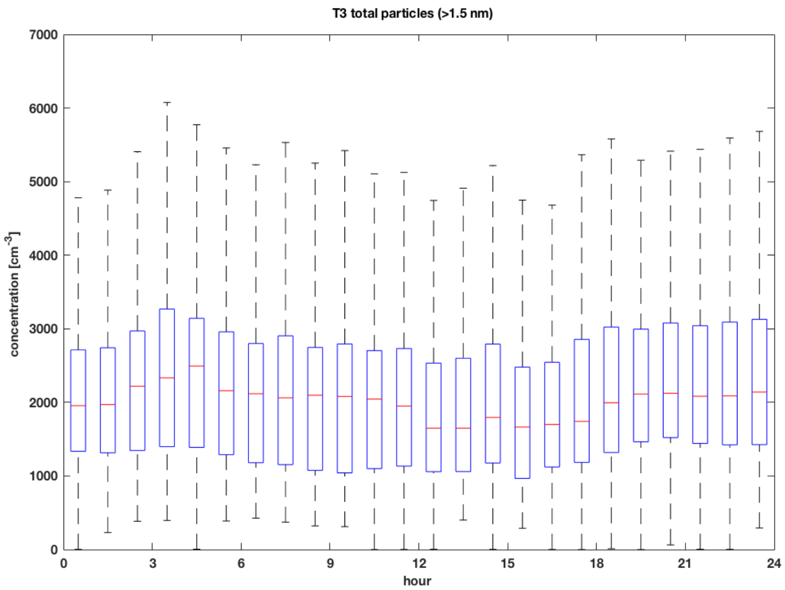

Fig 8. The diel cycle of particles bigger than 1.5 nm measured by the PSM during the dry season at the pasture site is shown. In total, 38 days of data were used. The data show hourly median concentrations, the boxes represent the 25th and 75th percentiles and the whiskers are 1.5 x IQR (interquartile range), data points beyond the whiskers are considered outliers.

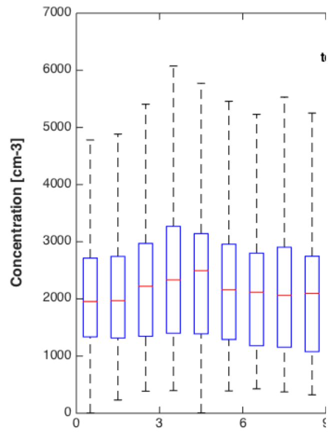

Deleted:

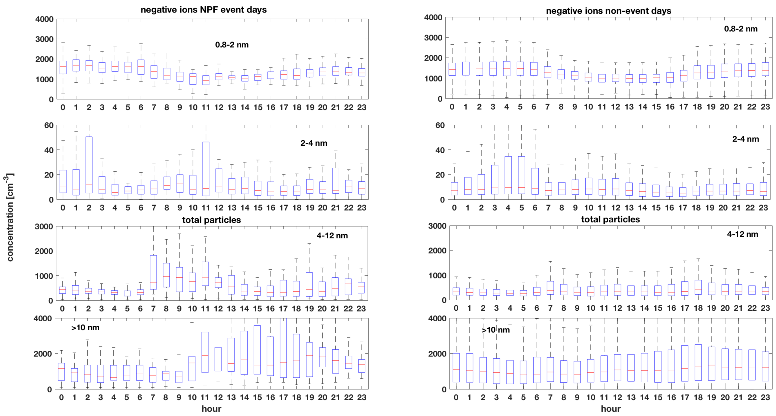

Figure 9. The median diel cycles of cluster ions (0.8 – 2nm), intermediate ions (2 – 4 nm), large (4 – 12 nm) neutral particles, and total particles (>10 nm) for new particle formation event days (left) and non-event days (right) are shown. The boxes show the 25th -75th percentiles and the whiskers are 1.5 x IQR (interquartile range), data points beyond the whiskers are considered outliers.

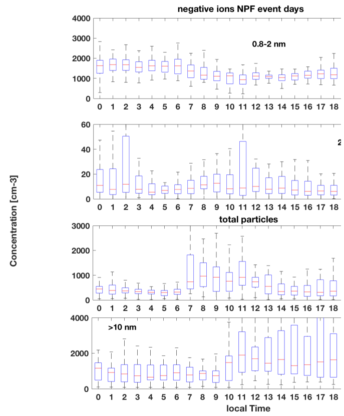

Deleted:

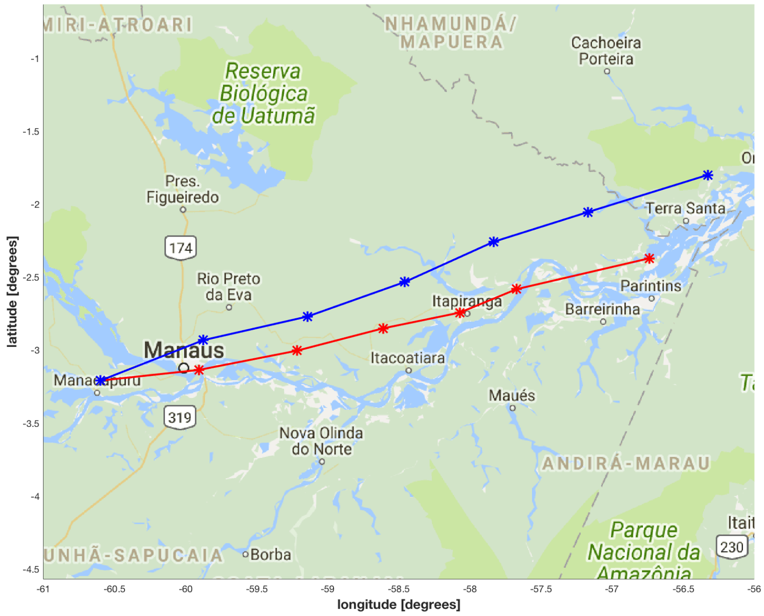

Figure 10: median back trajectories for NPF (blue) and non-event (red) days are shown. The trajectories were calculated 24hours backwards arriving at 09:00 local time at 500 m a.s.l. at the open pasture measurement site.

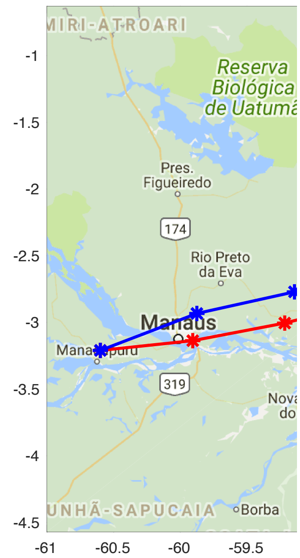

Deleted:

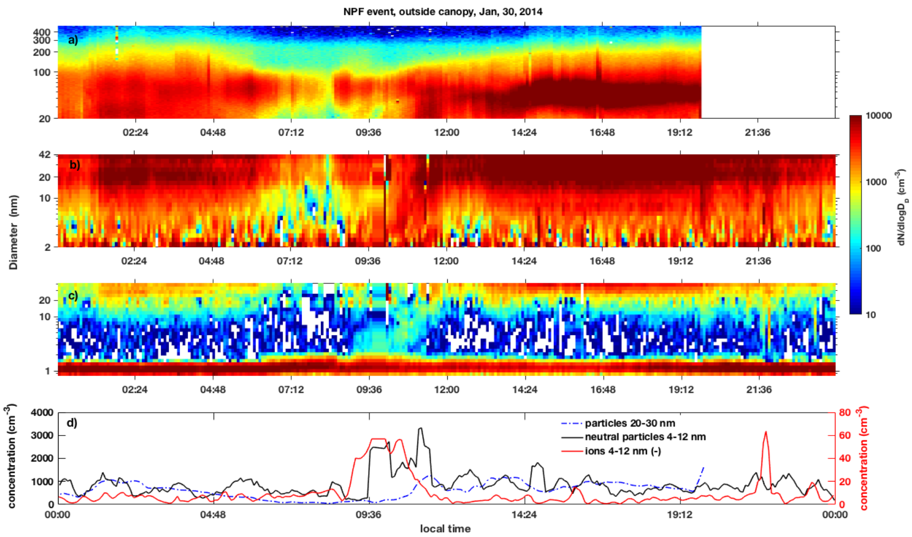

Figure 11. One example of an NPF event day, as observed at the open pasture (T3) site. (a) shows the surface Figure from the SMPS, (b) and (c) show the surface Figures from the NAIS, (b) for neutral particles and (c) for negative ions. The color code indicates the measured concentrations. Panel (d) shows concentrations for the 20-30nm size range from the SMPS on the left-hand axis (blue dashed line). The solid red line shows the 4-12 nm negative ion concentration on the right-hand axis and the solid black line the 4-12 nm neutral particle concentration on the left-hand axis.